engineering proceedings

MDPI

Proceeding Paper

Effects of Copper Substitution in Methylammonium-Based Perovskite Solar Cells †

Riku Okumura [1], Takeo Oku [1,*], Atsushi Suzuki [1], Sakiko Fukunishi [2], Tomoharu Tachikawa [2] and Tomoya Hasegawa [2]

[1] Department of Materials Chemistry, The University of Shiga Prefecture, 2500 Hassaka, Hikone, Shiga 522-8533, Japan
[2] Osaka Gas Chemicals Co., Ltd., 5-11-61 Torishima, Konohana-ku, Osaka 554-0051, Japan
* Correspondence: oku@mat.usp.ac.jp; Tel.: +81-749-28-8368
† Presented at the 4th International Electronic Conference on Applied Sciences, 27 October–10 November 2023; Available online: https://asec2023.sciforum.net/.

Abstract: The addition of copper bromide to the perovskite precursor solutions increased the conversion efficiencies of the devices. On the other hand, the short-circuit current densities decreased with an increase in the added amounts of copper (Cu). From first-principles calculations, the partial substitution of lead with Cu resulted in the formation of a Cu d orbital energy level in the forbidden band, which worked as a recombination center, causing the generated carriers to disappear. Experiments and calculations show the effects of Cu substitution on the electronic structures and the ability of the addition of Cu compounds to further improve the device performance.

Keywords: copper; first-principles calculations; perovskite; solar cell

Citation: Okumura, R.; Oku, T.; Suzuki, A.; Fukunishi, S.; Tachikawa, T.; Hasegawa, T. Effects of Copper Substitution in Methylammonium-Based Perovskite Solar Cells. *Eng. Proc.* **2023**, *56*, 47. https://doi.org/10.3390/ASEC2023-15403

Academic Editor: Letizia De Maria

Published: 27 October 2023

1. Introduction

Perovskite materials with excellent photovoltaic properties have been studied using a wide variety of approaches, including first-principles calculations [1–5], machine learning [6–10], and device characteristics simulations [11–15], in addition to experiments [16–22]. Although the conversion efficiency and stability of perovskite solar cells are gradually improving, most perovskite materials with excellent performance contain toxic Pb. In order to reduce the perovskite solar cells' toxicity for commercialization, alternative elements to Pb are being investigated [23–29]. In previous studies investigating the effect of Cu compound addition in methylammonium (MA)- or Cs-based perovskites, it was reported that the additions of small amounts of Cu to the perovskite precursor solution increased the grain size and improved the film quality, which contributed to improved device properties [30–34]. Furthermore, the combination of Cu with alkali metals or organic cations more stable than MA improved the conversion efficiency and stability of perovskite solar cells [35–38].

In this study, the effects of the addition of Cu compounds to the perovskite precursor solution and the substitution of Pb with Cu on the device properties and electronic structure were investigated [39]. The amount of Cu added was varied in the range of 0, 1, 2, 3, and 12.5%, and the current–voltage characterization and X-ray diffraction measurements were performed. In addition, first-principles calculations were performed to determine the effect of Cu substitution in methylammonium-based perovskite crystals from the band structure and partial density of states.

2. Device Fabrication and Computational Conditions

The structure of the fabricated perovskite solar cell is fluorine-doped tin oxide glass/compact TiO_2/mesoporous TiO_2/$CH_3NH_3PbI_3$/spiro-OMeTAD/Au. $CuBr_2$ was used as the Cu compound to be added to the perovskite precursor solution, with 0% Cu as the

standard device and different Cu additions in the range of 1, 2, 3, and 12.5%. The details of the experimental methods are described in the previous papers [35].

A 2 × 2 × 2 supercell was built, and one of the eight B-sites was substituted with Cu to produce a structural model of $MAPb_{0.875}Cu_{0.125}I_3$. The energy gap and carrier effective mass were calculated from the band structure, and the information on orbitals was obtained from the partial density of states (pDOS). The details of the calculation method are described in the previous papers [39].

3. Results and Discussion

Figure 1 shows the cell parameters as a function of the amount of Cu compound added to the perovskite precursor solution. Table 1 shows the values of the cell parameters obtained from the current–voltage characterization. The highest open circuit voltage (V_{OC}) and fill factor (*FF*) were obtained when 2% Cu was added, and the conversion efficiency was higher than that of standard devices. The short-circuit current density (J_{SC}) tended to decrease with an increase in the Cu addition, and the conversion efficiency decreased compared to the standard device when the Cu content exceeded 2%.

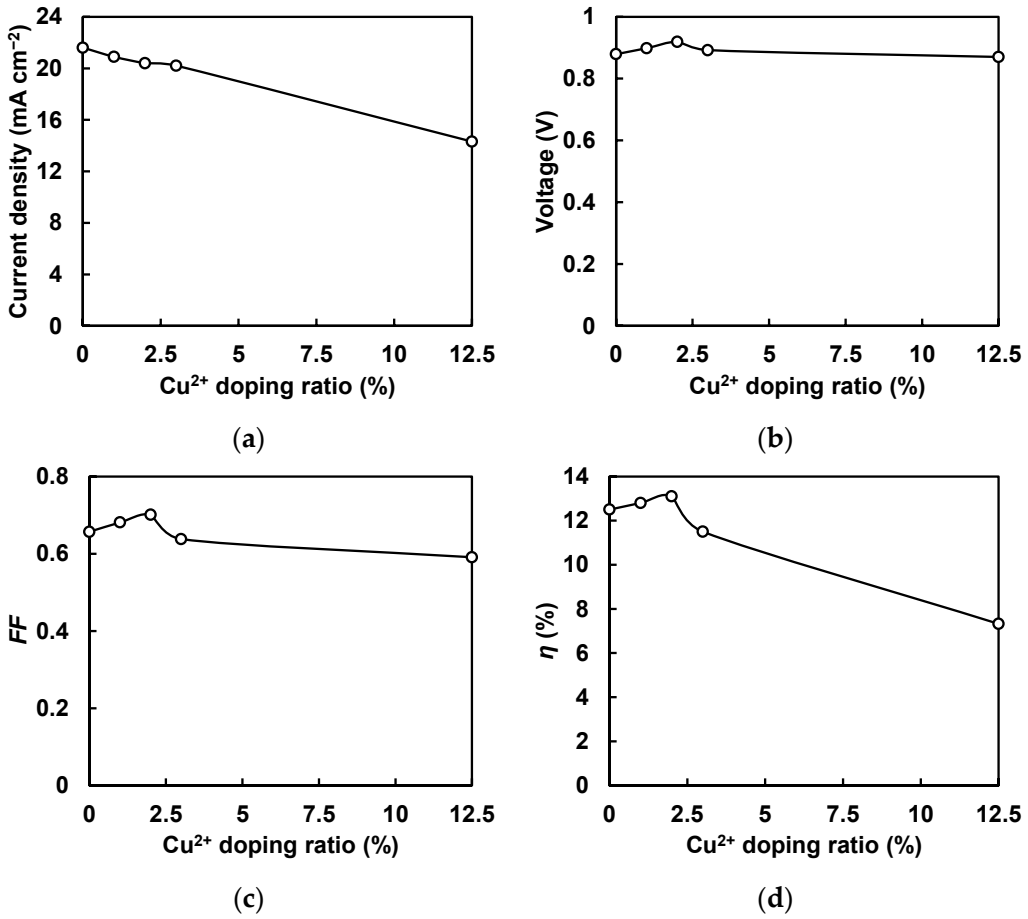

Figure 1. (**a**) J_{SC}, (**b**) V_{OC}, (**c**) *FF*, and (**d**) η values as a function of Cu^{2+} doping ratio.

Table 1. Device properties of perovskite solar cells.

Cu^{2+} (%)	J_{SC} (mA cm^{-2})	V_{OC} (V)	*FF*	R_S (Ω cm^2)	R_{Sh} (Ω cm^2)	η (%)	η_{ave} (%)	E_g (eV)
0	21.6	0.879	0.657	4.04	1664	12.5	10.4	1.55
1	20.9	0.898	0.681	3.49	1526	12.8	11.6	1.55
2	20.4	0.919	0.701	3.03	1507	13.1	11.7	1.56
3	20.2	0.892	0.638	4.85	1213	11.5	10.5	1.56
12.5	14.3	0.870	0.591	5.07	621	7.33	6.07	1.60

Table 2 shows the results of the X-ray diffraction pattern analysis. The crystallite size increased with the addition of Cu to the precursor solution, with 2% Cu showing the highest conversion efficiency and the highest perovskite (100) plane orientation. The increase in the lattice parameter with the addition of small amounts of Cu was attributed to the lattice distortion due to Cu substitution. For 12.5% Cu, the ionic radius of Cu is smaller than that of Pb; thus, the lattice shrank as more Cu was incorporated into the perovskite crystals.

Table 2. Parameters obtained from X-ray diffraction measurements.

Cu^{2+} (%)	I_{100}/I_{210}	Lattice Parameter (Å)	Crystallite Size (Å)
0	3.4	6.267(0)	394
1	3.7	6.269(1)	549
2	4.6	6.268(0)	663
3	4.2	6.268(1)	548
12.5	2.2	6.243(0)	625

First-principles calculations were performed to investigate the cause of the decrease in J_{SC} with an increase in the Cu addition. Figure 2 shows the calculated band structure and density of partial states. Table 3 shows the values of the parameters obtained from the first-principles calculations. From Figure 2c, the valence and conduction bands are composed of I p and Pb p orbitals, respectively. When Pb is partially substituted by Cu, the band gap decreases due to the lower energy of the Pb p orbital. Furthermore, an energy level of the Cu d orbital was formed in the forbidden band. Considering the experimental results, the energy level of the Cu d orbital worked as a defect level, causing the loss of the generated carriers and the reduction in the J_{SC}. In the absence of Cu, electrons are excited from the I p orbital to the Pb p orbital. In the presence of Cu, electrons can be excited from the I p orbital to the Cu d or Pb p orbital, resulting in two patterns of excitation processes. Despite the increase in the excitation probability, the decrease in device properties with an increase in the Cu addition means that it is difficult to extract electrons excited from the I p orbital and trapped in the Cu d orbital as charge carriers. Experimental and computational results indicate that the Cu substitution has a negative effect on the electronic structure and that the defect levels formed in the forbidden bands reduce the J_{SC}. Therefore, the enhancement of device properties by the addition of Cu compounds to the precursor solution is attributed to improvements in the microstructure of the perovskite film, such as an increase in crystallite size and perovskite crystal (100) plane orientation.

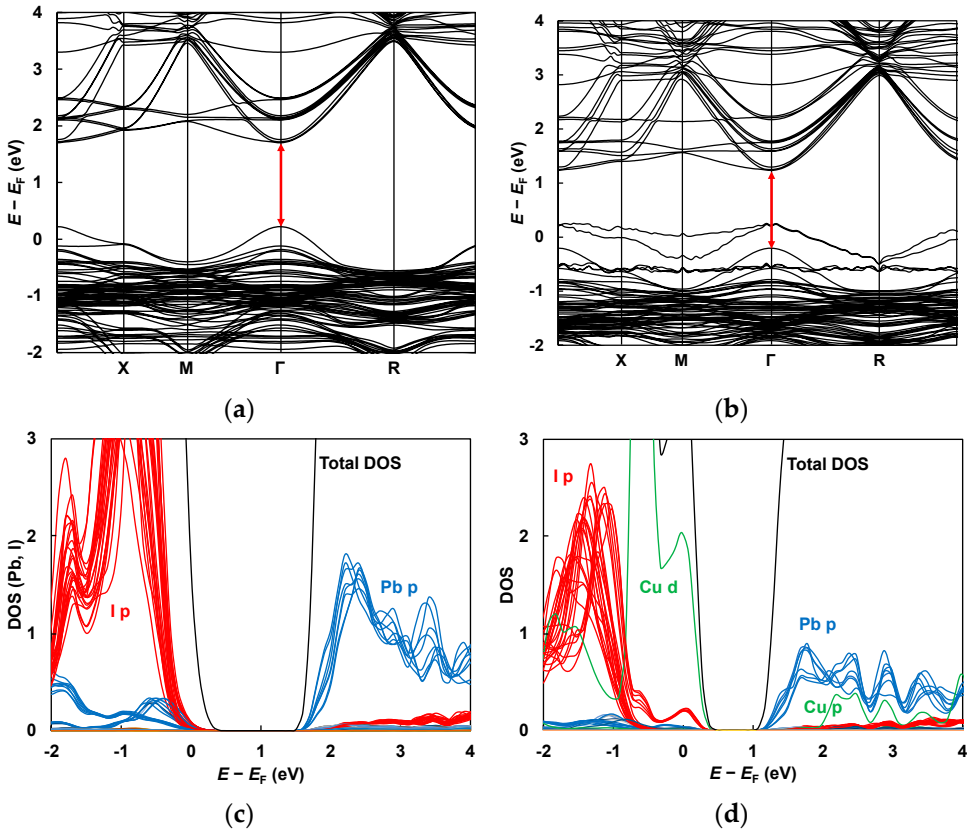

Figure 2. (**a**,**b**) Calculated band structures and (**c**,**d**) DOS of $MAPbI_3$ and $MAPb_{0.875}Cu_{0.125}I_3$, respectively. The red arrows in the band structures indicate the band gaps.

Table 3. Parameters obtained from first-principles calculations. The * means effective mass.

Model	Total Energy (eV cell^{-1})	Energy Gap (eV)	m_e^*/m_0 Pb	m_h^*/m_0 I	m_h^*/m_0 Cu	Contribution of Transition (%)	Oscillator Strength
$MAPbI_3$	−3495	1.480	0.229	0.208	–	16.7	0.0168
Cu 12.5%	−3363	1.438	0.240	0.239	0.355	62.2	0.0287

4. Conclusions

The addition of 2% Cu to the perovskite precursor solution improved the V_{OC} and *FF* and enhanced the conversion efficiency of the device. The calculated band structure and density of partial states indicate that the substitution of Pb for Cu has a negative effect on the electronic structure, with the formation of Cu d orbital energy levels in the forbidden band causing carrier recombination and lowering of the J_{SC}. Therefore, it is difficult to adopt Cu as a replacement element for Pb, but the addition of small amounts of Cu compounds to the perovskite precursor solution was shown to contribute to the further enhancement of device properties.

Author Contributions: Conceptualization, R.O.; methodology, R.O., T.O. and A.S.; formal analysis, R.O. and T.O.; investigation, R.O. and T.O.; resources, S.F., T.T. and T.H.; data curation, R.O. and T.O.; writing—original draft preparation, R.O. and T.O.; writing—review and editing, R.O., T.O., A.S., S.F., T.T. and T.H.; project administration, T.O.; funding acquisition, T.O. All authors have read and agreed to the published version of the manuscript.

Funding: This research was partly funded by Japan Society for the promotion of Science as a Grant-in-Aid for Scientific Research (C) 21K04809.

Institutional Review Board Statement: Not applicable.

Informed Consent Statement: Not applicable.

Data Availability Statement: Data are contained within the article.

Conflicts of Interest: Authors S.F., T.T., and T.H. were employed by the company Osaka Gas Chemicals Co., Ltd. The remaining authors declare that the research was conducted in the absence of any commercial or financial relationships that could be construed as a potential conflict of interest.

References

1. Hossain, M.K.; Arnab, A.A.; Das, R.C.; Hossain, K.M.; Rubel, M.H.K.; Rahman, M.F.; Bencherif, R.H.; Emetere, M.E.; Mohammed, M.K.A.; Pandey, R. Combined DFT, SCAPS-1D, and wxAMPS frameworks for design optimization of efficient Cs_2BiAgI_6-based perovskite solar cells with different charge transport layers. *RSC Adv.* **2022**, *12*, 35002. [CrossRef]
2. Han, S.; Guan, L.; Yin, T.; Zhang, J.; Guo, J.; Chen, X.; Li, X. Unveiling the roles of halogen ions in the surface passivation of $CsPbI_3$ perovskite solar cells. *Phys. Chem. Chem. Phys.* **2022**, *24*, 10184–10192. [CrossRef]
3. Gao, Z.; Mao, G.; Chen, S.; Bai, Y.; Gao, P.; Wu, C.; Gates, I.D.; Yang, W.; Ding, X.; Yao, J. High throughput screening of promising lead-free inorganic halide double perovskites via first-principles calculations. *Phys. Chem. Chem. Phys.* **2022**, *24*, 3460–3469. [CrossRef]
4. Manzoor, M.; Iqbal, M.W.; Imran, M.; Noor, N.A.; Mahmood, A.; Alanazi, Y.M.; Aftab, S. Probing direct bandgap of double perovskites Rb_2LiTlX_6 (X = Cl, Br) and optoelectronic characteristics for Solar cell applications: DFT calculations. *J. Mater. Res. Technol.* **2022**, *18*, 4775–4785. [CrossRef]
5. Guo, J.; Sun, J.; Hu, L.; Fang, S.; Ling, X.; Zhang, X.; Wang, Y.; Huang, H.; Han, C.; Cazorla, C.; et al. Indigo: A Natural Molecular Passivator for Efficient Perovskite Solar Cells. *Adv. Energy Mater.* **2022**, *12*, 2200537. [CrossRef]
6. Mammeri, M.; Dehimi, L.; Bencherif, H.; Pezzimenti, F. Paths towards high perovskite solar cells stability using machine learning techniques. *Sol. Energy* **2023**, *249*, 651–660. [CrossRef]
7. Hussain, W.; Sawar, S.; Sultan, M. Leveraging machine learning to consolidate the diversity in experimental results of perovskite solar cells. *RSC Adv.* **2023**, *13*, 22529–22537. [CrossRef]
8. Liu, Z.; Rolston, N.; Flick, A.C.; Colburn, T.W.; Ren, Z.; Dauskardt, R.H.; Buonassisi, T. Machine learning with knowledge constraints for process optimization of open-air perovskite solar cell manufacturing. *Joule* **2022**, *6*, 834–849. [CrossRef]
9. Parikh, N.; Karamta, M.; Yadav, N.; Tavakoli, M.M.; Prochowicz, D.; Akin, S.; Kalam, A.; Satapathi, S.; Yadav, P. Is machine learning redefining the perovskite solar cells? *J. Energy Chem.* **2022**, *66*, 74–90. [CrossRef]
10. Hu, Y.; Hu, X.; Zhang, L.; Zheng, T.; You, J.; Jia, B.; Ma, Y.; Du, X.; Zhang, L.; Wang, J.; et al. Machine-learning modeling for ultra-stable high-efficiency perovskite solar cells. *Adv. Energy Mater.* **2022**, *12*, 2201463. [CrossRef]
11. Rawa, M.; Al-Turki, Y.; Sindi, H.; Calasan, M.; Ali, Z.M.; Aleem, S.H.E.A. Current-voltage curves of planar heterojunction perovskite solar cells—Novel expressions based on Lambert W function and Special Trans Function Theory. *J. Adv. Res.* **2023**, *44*, 91–108. [CrossRef]
12. Omrani, M.; Keshavarzi, R.; Abdi-Jalebi, M.; Gao, P. Impacts of plasmonic nanoparticles incorporation and interface energy alignment for highly efcient carbon-based perovskite solar cells. *Sci. Rep.* **2022**, *12*, 5367. [CrossRef]
13. Al-Mousoi, A.K.; Mohammed, M.K.A.; Pandey, R.; Madan, J.; Dastan, D.; Ravi, G.; Sakthivel, P.; Anandha Babu, G. Simulation and analysis of lead-free perovskite solar cells incorporating cerium oxide as electron transporting layer. *RSC. Adv.* **2022**, *12*, 32365–32373. [CrossRef]
14. Farhadi, B.; Zabihi, F.; Tebyetekerwa, M.; Lugoloobi, I.; Liu, A. Influence of the anode buffer layer materials and the light radiation power on the efficiency of a planar p-i-n perovskite solar cell: Theory and simulation. *Photonics Energy* **2022**, *12*, 015503. [CrossRef]
15. Obraztsova, A.A.; Barettin, D.; Furasova, A.D.; Voroshilov, P.M.; Maur, M.A.; Orsini, A.; Makarov, S.V. Light-trapping electrode for the efficiency enhancement of bifacial perovskite solar cells. *Nanomaterials* **2022**, *12*, 3210. [CrossRef]
16. Li, G.; Su, Z.; Canil, L.; Hughes, D.; Aldamasy, M.H.; Dagar, J.; Trofimov, S.; Wang, L.; Zuo, W.; Jeronimo-Rendon, J.J.; et al. Highly efficient p-i-n perovskite solar cells that endure temperature variations. *Science* **2023**, *379*, 399–403. [CrossRef]
17. Jiang, Q.; Tong, J.; Scheidt, R.A.; Wang, X.; Louks, A.E.; Xian, Y.; Tirawat, R.; Palmstrom, A.F.; Hautzinger, M.P.; Harvey, S.P.; et al. Compositional texture engineering for highly stable wide-bandgap perovskite solar cells. *Science* **2022**, *378*, 1295–1300. [CrossRef]
18. Li, Z.; Li, B.; Wu, X.; Sheppard, S.A.; Zhang, S.; Gao, D.; Long, N.J.; Zhu, Z. Organometallic-functionalized interfaces for highly efficient inverted perovskite solar cells. *Science* **2022**, *376*, 416–420. [CrossRef]
19. Li, H.; Zhou, J.; Tan, L.; Li, M.; Jiang, C.; Wang, S.; Zhao, X.; Liu, Y.; Zhang, Y.; Ye, Y.; et al. Sequential vacuum-evaporated perovskite solar cells with more than 24% efficiency. *Sci. Adv.* **2022**, *8*, eabo7422. [CrossRef]
20. Jiang, Q.; Tong, J.; Xian, Y.; Kerner, R.A.; Dunfield, S.P.; Xiao, C.; Scheidt, R.A.; Kuciauskas, D.; Wang, X.; Hautzinger, M.P.; et al. Surface reaction for efficient and stable inverted perovskite solar cells. *Nature* **2022**, *611*, 278–283. [CrossRef]
21. Peng, J.; Kremer, F.; Walter, D.; Wu, Y.; Ji, Y.; Xiang, J.; Liu, W.; Duong, T.; Shen, H.; Lu, T.; et al. Centimetre-scale perovskite solar cells with fill factors of more than 86 per cent. *Nature* **2022**, *601*, 573–578. [CrossRef]
22. Zhang, D.; Li, D.; Hu, Y.; Mei, A.; Han, H. Degradation pathways in perovskite solar cells and how to meet international standards. *Com. Mater.* **2022**, *3*, 58. [CrossRef]

23. Ji, F.; Boschloo, G.; Wang, F.; Gao, F. Challenges and progress in lead-free halide double perovskite solar cells. *Sol. RRL* **2023**, *7*, 2201112. [CrossRef]
24. Pering, S.R. The diferences in crystal structure and phase of lead-free perovskite solar cell materials. *Discov. Mater.* **2023**, *3*, 23. [CrossRef]
25. Nishat, M.; Hossain, M.K.; Hossain, M.R.; Khanom, S.; Ahmed, F.; Hossain, M.A. Role of metal and anions in organo-metal halide perovskites $CH_3NH_3MX_3$ (M: Cu, Zn, Ga, Ge, Sn, Pb; X: Cl, Br, I) on structural and optoelectronic properties for photovoltaic applications. *RSC Adv.* **2022**, *12*, 13281. [CrossRef]
26. Pering, S.R.; Gillions, H.; Kuznetsov, T.; Zhang, W.; Yendall, K.; Togay, M. Investigation of solution-based synthesis of non-toxic perovskite materials using Mg, Ca, Mn, Fe, Cu, and Zn as the B-site cation for photovoltaic applications. *J. Mater. Chem. C* **2022**, *10*, 14722. [CrossRef]
27. Schileo, G.; Grancini, G. Lead or no lead? Availability, toxicity, sustainability and environmental impact of lead-free perovskites solar cells. *J. Mater. Chem. C* **2021**, *9*, 67. [CrossRef]
28. Xu, J.; Maxwell, A.; Wei, M.; Wang, Z.; Chen, B.; Zhu, T.; Sargent, E.H. Defect tolerance of mixed B-Site organic-inorganic halide perovskites. *ACS Energy Lett.* **2021**, *6*, 4220–4227. [CrossRef]
29. Tian, J.; Xue, Q.; Yao, Q.; Li, N.; Brabec, C.J.; Yip, H.L. Inorganic halide perovskite solar cells: Progress and challenges. *Adv. Energy Mater.* **2020**, *10*, 2000183. [CrossRef]
30. Jahandar, M.; Heo, J.H.; Song, C.E.; Kong, K.J.; Shin, W.S.; Lee, J.C.; Im, S.H.; Moon, S.J. Highly efficient metal halide substituted $CH_3NH_3I(PbI_2)_{1-X}(CuBr_2)_X$ planar perovskite solar cells. *Nano Energy* **2016**, *27*, 330–339. [CrossRef]
31. Tanaka, H.; Ohishi, Y.; Oku, T. Effects of Cu addition to perovskite $CH_3NH_3PbI_{3-x}Cl_x$ photovoltaic devices with hot airflow during spin-coating. *Jpn. J. Appl. Phys.* **2018**, *57*, 08RE10. [CrossRef]
32. Tanaka, H.; Ohishi, Y.; Oku, T. Fabrication and characterization of the copper bromides-added $CH_3NH_3PbI_{3-x}Cl_x$ perovskite solar cells. *Synth. Met.* **2018**, *244*, 128–133. [CrossRef]
33. Wang, K.L.; Wang, R.; Wang, Z.K.; Li, M.; Zhang, Y.; Ma, H.; Liao, L.S.; Yang, Y. Tailored phase transformation of $CsPbI_2Br$ films by copper(II) bromide for high-performance all-inorganic perovskite solar cells. *Nano Lett.* **2019**, *19*, 5176–5184. [CrossRef]
34. Asakawa, Y.; Oku, T.; Kido, M.; Suzuki, A.; Okumura, R.; Okita, M.; Fukunishi, S.; Tachikawa, T.; Hasegawa, T. Fabrication and characterization of $SnCl_2$- and CuBr-added perovskite photovoltaic devices. *Technologies* **2022**, *10*, 112. [CrossRef]
35. Ueoka, N.; Oku, T.; Suzuki, A. Additive effects of alkali metals on Cu-modified $CH_3NH_3PbI_{3-\delta}Cl_\delta$ photovoltaic devices. *RSC Adv.* **2019**, *9*, 24231. [CrossRef]
36. Ueoka, N.; Oku, T. Effects of co-addition of sodium chloride and copper(II) bromide to mixed-cation mixed-halide perovskite photovoltaic devices. *ACS Appl. Energy Mater.* **2020**, *3*, 7272–7283. [CrossRef]
37. Ueoka, N.; Oku, T.; Suzuki, A. Effects of doping with Na, K, Rb, and formamidinium cations on $(CH_3NH_3)_{0.99}Rb_{0.01}Pb_{0.99}Cu_{0.01}I_{3-x}(Cl, Br)_x$ perovskite photovoltaic cells. *AIP Adv.* **2020**, *10*, 125023. [CrossRef]
38. Okumura, R.; Oku, T.; Suzuki, A.; Okita, M.; Fukunishi, S.; Tachikawa, T.; Hasegawa, T. Effects of adding alkali metals and organic cations to Cu-based perovskite solar cells. *Appl. Sci.* **2022**, *12*, 1710. [CrossRef]
39. Okumura, R.; Oku, T.; Suzuki, A.; Fukunishi, S.; Tachikawa, T.; Hasegawa, T. First-principles calculation analysis and photovoltaic properties of Cu compoundadded perovskite solar cells. *Jpn. J. Appl. Phys.* **2023**, *62*, SK1029. [CrossRef]